Mechanical characterization of GdBCO/Ag and YBCO single grains fabricated by top-seeded melt growth at 77 and 300 K

2014 Supercond. Sci. Technol. 27 115011

(http://iopscience.iop.org/0953-2048/27/11/115011)

OPEN ACCESS

Made open access 20 October 2014

IOP Publishing

Superconductor Science and Technology

Supercond. Sci. Technol. **27** (2014) 115011 (11pp)

doi:10.1088/0953-2048/27/11/115011

Mechanical characterization of GdBCO/Ag and YBCO single grains fabricated by top-seeded melt growth at 77 and 300 K

K Konstantopoulou[1], Y H Shi[2], A R Dennis[2], J H Durrell[2], J Y Pastor[1] and D A Cardwell[2]

[1] Departamento de Ciencia de Materiales, Universidad Politécnica de Madrid, E. T. S. de Ingenieros de Caminos, C/Prof. Aranguren s/n, E28040 Madrid, Spain
[2] Department of Engineering, Bulk Superconductivity Group, University of Cambridge, Trumpington Street, Cambridge, CB2 1PZ, UK

E-mail: konstantina@mater.upm.es

Received 16 July 2014, revised 8 September 2014
Accepted for publication 10 September 2014
Published 8 October 2014

Abstract

YBaCuO and GdBaCuO + 15 wt% Ag large, single-grain, bulk superconductors have been fabricated via the top-seeded, melt-growth (TSMG) process using a generic NdBCO seed. The mechanical behavior of both materials has been investigated by means of three-point bending (TPB) and transversal tensile tests at 77 and 300 K. The strength, fracture toughness and hardness of the samples were studied for two directions of applied load to obtain comprehensive information about the effect of microstructural anisotropy on the macroscopic and microscopic mechanical properties of these technologically important materials. Splitting (Brazilian) tests were carried out on as-melt-processed cylindrical samples following a standard oxygenation process and with the load applied parallel to the growth-facet lines characteristic of the TSMG process. In addition, the elastic modulus of each material was measured by three different techniques and related to the microstructure of each sample using optical microscopy. The results show that both the mechanical properties and the elastic modulus of both YBCO and GdBCP/Ag are improved at 77 K. However, the GdBCO/Ag samples are less anisotropic and exhibit better mechanical behavior due to the presence of silver particles in the bulk, superconducting matrix. The splitting tensile strength was determined at 77 K and both materials were found to exhibit similar behavior, independently of their differences in microstructure.

Keywords: mechanical properties, HTS bulk materials, microstructure

(Some figures may appear in colour only in the online journal)

1. Introduction

Bulk, melt-processed high-temperature superconducting (HTS) materials exhibit enhanced magnetic properties compared to conventional permanent magnets due primarily to their ability to trap large magnetic fields at temperatures that can be achieved using commercially available, cryo-cooler technology. This ability makes bulk HTS, such as (RE)BCO (where RE is a rare-earth element) particularly attractive for a variety of large-scale applications, including bulk magnets, flywheel energy storage systems, magnetic bearings, magnetic separators and fault current limiters [1, 2]. YBCO and GdBCO have emerged over the past 20 years within the (RE)BCO family of bulk HTS as the most promising for practical applications, and numerous studies have been performed to improve the single-grain fabrication process for these materials [3, 4]. One of the most well-known methods is the top-seeded melt-growth (TSMG) process, which has been used to produce high performance (RE)BCO samples [5, 6]. GdBCO generally exhibits higher critical current density, J_c, in the presence of applied magnetic fields than YBCO, which makes it more suitable for many applications [7, 8]. Unfortunately, the world record fields of up to

17.6 T that have been produced recently by these remarkable materials are limited, ultimately, by the mechanical properties of the bulk superconductor [9, 10]. The Lorentz force generated within a bulk superconductor in the presence of a large magnetic field is sufficient to cause internal fracture of the single grain, although relatively little research has been performed on the magnitude of the stresses generated during the magnetization process. Bulk (RE)BCO single grains tend to fracture when the internal electromagnetic stresses exceed values of 10–-30 MPa [11]. Although J_c and the irreversibility field, H_{irr}, are higher for GdBCO than YBCO, the latter remains a very good candidate for a variety of applications and has consequently been the subject of numerous studies on its superconducting and mechanical properties [12–15]. Relatively few studies, on the other hand, have been performed on the mechanical behavior of GdBCO single grains. In this work, the mechanical properties of GdBCO/Ag and YBCO single-grain superconductors fabricated by TSMG using a generic NdBCO seed have been studied and compared. The mechanical behavior of the bulk samples has been measured by both three-point bending and splitting tests. The Brazilian (splitting) test is an experimental method applied widely to characterize both structural and functional materials, such as concrete [16], graphite [17] and functional ceramics [18]. This method enables as-processed, annealed single grains to be tested without the additional need for additional processing into smaller sub-specimens. It is also informative to compare the experimental results with the magnitude of the stresses produced under the conditions of a high-trapped magnetic field. In this way, it is possible to determine if a particular material can withstand the expected maximum tensile stress in service in high-field applications.

The main aim of this work was to perform a thorough characterization of the mechanical properties of GdBCO/Ag and YBCO bulk, melt-processed samples at 77 and 300 K and to determine the maximum tensile strength of these materials at 77 K. The strength-limiting features of the sample microstructure have been identified as part of this investigation.

2. Experimental procedure

2.1. Processing of GdBCO/Ag and YBCO single grains

Cylindrical, single-grain samples of YBCO and GdBCO/Ag were batch-processed by the top-seeded, melt-growth (TSMG) technique [19]. Oxide powders were mixed together in the desired composition and an NdBCO generic seed was used to nucleate and grow single grains of both materials [20]. A standard composition of 70 wt% Y-123, 30 wt% Y-211 and 1 wt% CeO_2 was used for YBCO. Precursor powders of composition Gd-123 at 75 wt%, Gd-211 at 25 wt% and an excess of 15 wt% Ag_2O, 1 wt% BaO_2 and 0.1 wt% Pt were used to process the GdBCO/Ag samples. Different furnace profiles were applied for GdBCO/Ag and YBCO, taking in account the different melting temperatures of the two (RE)BCO compounds, T_m (YBCO: 1005 °C, GdBCO/Ag: 1000 °C and GdBCO: 1030 °C). Six single-grain samples were processed for each compound (figure 1). The nominal dimensions of the cylindrical samples obtained for both materials following melt processing were 25 mm in diameter and 12 mm in height.

Figure 1. Batch-processed YBCO (left) and GdBCO/Ag (right) single-grain samples.

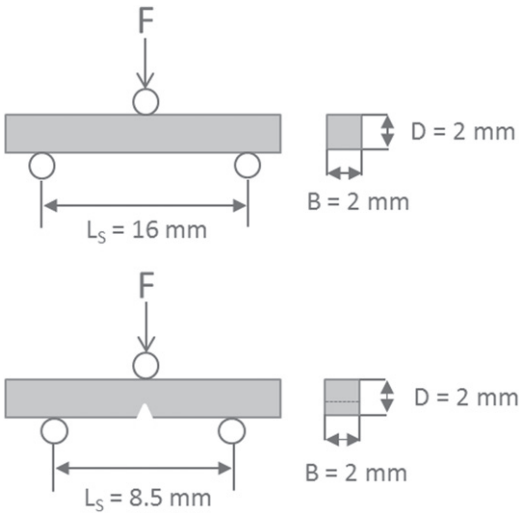

Figure 2. Schematic illustration of the three-point bending tests for evaluation of the flexural strength and fracture toughness.

2.2. Mechanical characterization

The YBCO and GdBCO/Ag samples were characterized via three-point bending tests to determine their flexural strength and fracture toughness. In order to check the effect of the microstructural anisotropy on the mechanical properties, all tests were performed for loading directions parallel to the *c*-axis and parallel to the *ab*-plane. The as-grown cylinders were cut with a diamond wire to obtain the desirable prismatic-shaped specimens for the three-point bending tests. The nominal dimensions of all the specimens measured were $2 \times 2 \times 20$ mm and the span between the test supports was 8.5 mm and 16 mm for fracture toughness and flexural strength measurements, respectively (figure 2).

All tests were carried out using an electromechanical testing machine (Instron 5866), with the applied load and the displacement of the loading point recorded constantly during the test with a load cell at 1000 ± 1 N.

The test device used at low (77 K) and room temperature was similar in both cases. The main difference between the two test conditions was that an additional cryogenic chamber

was attached to the electromechanical testing machine in the vicinity of the loading device in the low-temperature tests. The bottom of the vessel and its load application point were connected to the actuator and the load cell of the machine, respectively, via hollow bars of stainless steel to prevent excessive cooling of the measurement instrumentation during this test. The cryogenic chamber was coated with polyurethane and cryogenic foam to insulate the system and to maintain a constant temperature during the experiment. The cryogenic tests were performed by immersing the specimens in boiling liquid nitrogen (i.e. at a temperature of 77 K), with the temperature stabilized for around 10 min before each test was performed.

The level of liquid nitrogen in the cryogenic vessel was maintained throughout the low-temperature test by refilling as necessary to keep the specimen and part of the loading device completely immersed during the measurement. This process was monitored to ensure it did not affect either the measurement of the load or the displacement.

The positions of all test devices and specimens were fixed prior to cooling. A constant, compressive load of low magnitude (4 N) was applied throughout the cooling and measurement process to keep the system in balance and to avoid any movement of the sample or the supporting rollers and plates. The three-point bending tests were performed using displacement control at a constant, cross-head speed of 100 μm min^{-1}.

Flexural strength, σ_F, was calculated from the measured maximum load using established equations of materials strength [21]. The fracture toughness, K_{IC}, was calculated from the measured maximum load and the post-measurement notch length using the equation reported by Guinea *et al* [22].

Brazilian tests were carried out to obtain the splitting tensile strength, σ_T, of the two bulk materials under investigation. The samples tested were of cylindrical geometry (i.e. as-processed after annealing), and the load was distributed by two bearing strips positioned parallel to the growth facet lines characteristic of the TSMG process on the upper surface of the bulk, superconducting samples. The tests were performed at 77 K in a servohydraulic machine (INSTRON 8501) using a device designed specifically to center both the samples and the load-bearing strips. A schematic illustration of the Brazilian test arrangement is shown in figure 3. The splitting tensile strength was calculated from:

$$\sigma_T = \frac{2P}{\pi BD}, \quad (1)$$

where P is the maximum applied load, B is the thickness of the samples and D is the diameter of the cylinder under test.

Nanoindentation tests were performed at 300 K using an MTS Nano Indenter, CSM/LFM Control Unit, with a calibrated Berkovich tip indenter [23]. The depth of the indentation was constant for all measurements ($h = 1$ μm). The tests were carried out for the two loading directions described above with 25 indentation tests performed for each load condition. The surfaces of the samples were analyzed after testing using a scanning electron microscope (SEM) in order to investigate the micro-mechanisms responsible for the observed macroscopic mechanical behavior of each material.

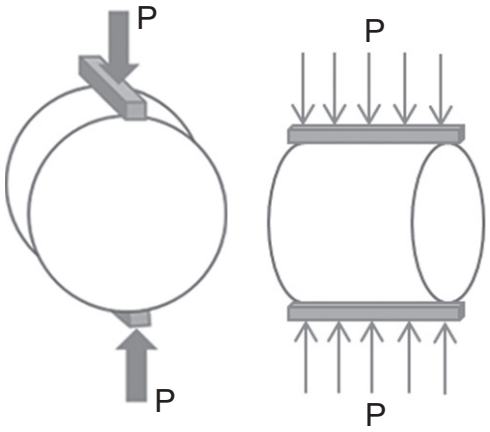

Figure 3. Schematic illustration of the Brazilian test for evaluation of tensile strength.

The Vickers hardness at 300 and 77 K was measured using an AKASHI, MVK-EIII instrument for the two loading directions using loads of 0.98 N and 9.80 N applied for a period of 15 s. The test was repeated 10 times under each test condition in order to obtain statistically significant data. A bespoke chamber was attached to the Vickers hardness tester in order to avoid any movement of the sample during the test to enable the measurements to be performed at 77 K.

Finally, the elastic modulus, E, of the single grains at 300 K was calculated using three different methods: (i) nanoindentation; (ii) vibrational resonance with a Grindosonic (Belgium) device; and (iii) the load-displacement curve of the three-point bending tests. For the latter, the elastic modulus was determined at both 300 K and 77 K from the linear zone of the stress–strain curves generated by the strength tests.

3. Results and discussion

3.1. Microstructure

The microstructure of both materials was studied to investigate the presence of different phases and associated characteristics that can affect the mechanical behavior of the samples. The *ab*-plane and the plane parallel to the *ab*-plane of each sample were exposed, embedded in resin and then polished using an abrasive paste of size 1 μm. The microstructures of the polished surfaces were revealed by etching with a solution of 95% of 2-butoxietanol and 5% of percloric acid at 0 °C prior to SEM investigation. The density of the YBCO and GdBCO/Ag single grains was 6.081 ± 0.009 g cm^{-3} and 7.039 ± 0.004 g cm^{-3}, respectively.

The Y-123 matrix and Y-211 secondary phase inclusions are readily apparent in figure 4. It can be seen that the Y-211 particles are relatively homogeneous and of size between 1 and 4 μm. Three phases are present in the GdBCO/Ag samples: the Gd-123 matrix and the Gd-211 and Ag particles. The silver particles are almost cylindrical in geometry with a

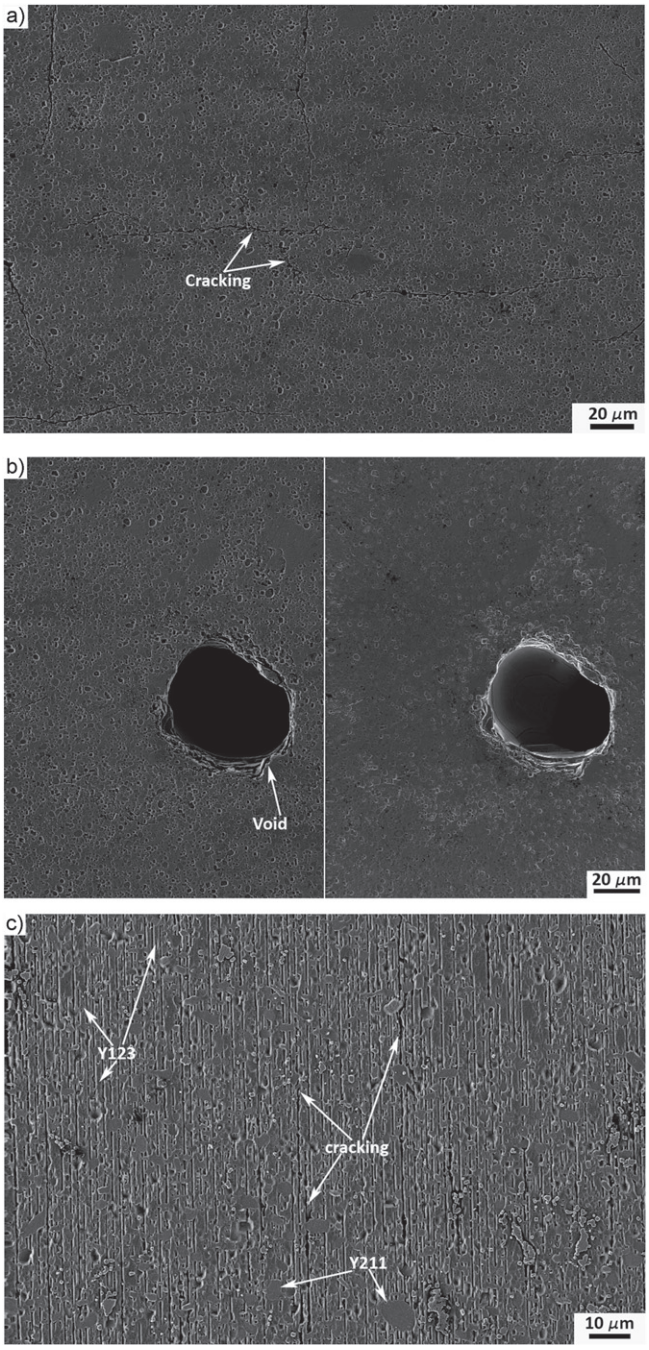

Figure 4. (a) Microstructure of the longitudinal section of the YBCO single grain. Microcracking perpendicular and parallel to the *ab*-plane can be seen in the micrograph. (b) Microstructure of the longitudinal section of the YBCO single grain. The size of the voids is indicated. (c) Microstructure of the transversal section of the YBCO single grain. The density of cracking parallel to the *ab*-plane and the secondary phase Y-211 are indicated.

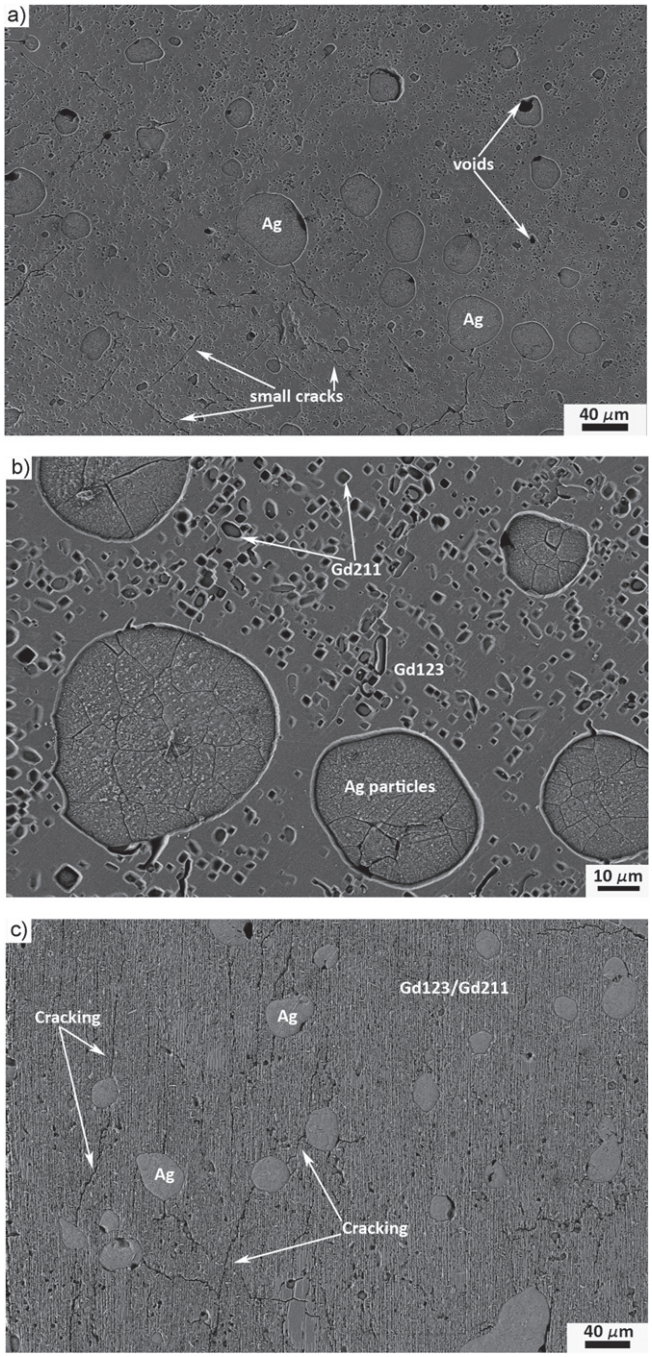

Figure 5. (a) Microstructure of the longitudinal section of the GdBCO/Ag 15 wt% single grain. Small cracks, voids and the size of Ag particles are indicated. (b) Microstructure of the longitudinal section of the GdBCO/Ag 15 wt% single grain. The secondary phase of Gd-211 and the size of Ag particles are indicated. (c) Microstructure of the transversal section of the GdBCO/Ag 15 wt% single grain. Cracking parallel to the *ab*-plane and around the Ag particles can be seen.

diameter of between 20 and 60 μm, whereas the Gd-211 phase is much smaller than the Y-211 phase in the YBCO single-grain matrix (figure 5).

The presence of microcracks and porosity has been observed previously in both YBCO and GdBCO/Ag single grains. GdBCO/Ag, however, typically contains lower porosity, and the voids are smaller than those of the YBCO samples. Microcracking parallel to the *ab*-plane generated during the oxygenation process is shown in figures 4 and 5. In addition, cracks oriented perpendicular to each other are also observed within the *ab*-plane. The propagation of the cracks occurs around, rather than through, the Y-211 and Gd-211 secondary phases, as has been reported previously [13].

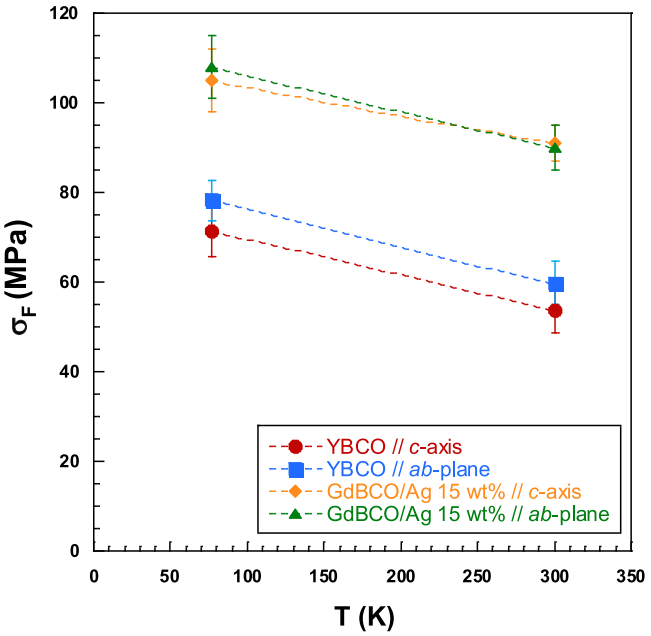

Figure 6. Variation of flexural strength as a function of temperature and test direction. Each point represents the mean value of the results of ten tests. The bars indicate the quadratic mean error.

Moreover, for GdBCO/Ag single grains, cracks that interconnect the Ag particles are present due to a mismatch in the thermal expansion coefficients of silver (1, 8×10^{-6} K^{-1}) and the bulk superconductor (10^{-5} K^{-1}).

3.2. Flexural strength

Three-point bending tests were performed to obtain the flexural strength of both YBCO and GdBCO/Ag single grains at 77 and 300 K, respectively. The direction of loading during the tests was either parallel to the *c*-axis or parallel to the *ab*-plane. Ten tests were performed for each loading direction and temperature, with the results presented in figure 6.

The mechanical behavior of both YBCO and GdBCO/Ag single grains was similar for both directions tested. An increase in σ_F of 30% is observed for YBCO at 77 K, independent of the loading direction, and between 15 and 20% (depending on the loading direction) for GdBCO/Ag.

However, the values of σ_F obtained for the GdBCO/Ag single grain are approximately 45% higher than those determined for YBCO at 77 K, compared to a difference of around 55% at room temperature. The addition of silver particles is well known to improve both the superconducting properties (by acting as pinning centers) and also the mechanical behavior [24] of the samples. Flexural strength has been observed in previous studies to depend on the loading direction [13]. The fracture mechanisms and the effects of the microstructural characteristics on the macroscopic mechanical properties of the samples were investigated with SEM by observation of the fracture surfaces of the samples following mechanical testing.

Figure 7 shows the brittle fracture surface of the YBCO sample at 77 K. The loading direction was parallel to the *c*-axis, with the resulting direction of propagation of cracks being perpendicular to the orientation of the pre-existing microcracks. The fracture characteristics of the grain and decohesion can be seen in the figure. The crack propagates initially perpendicular to the *ab*-plane (fracture of the grain) and then parallel to the *ab*-plane, resulting in decohesion. However, similar values of flexural strength were observed in both loading directions when the load was applied parallel to the *ab*-plane, resulting in the propagation of cracks through the pre-existing microcracks, as shown in figure 8. This occurred at both test temperatures, where the single grains exhibit similar, abrupt fracture surfaces. The propagation of cracks through the pre-existing microcracks would be reasonably expected to lower the flexural strength in this loading direction. According to the visual appearance of the fracture surfaces, however, decohesion of the grain is observed when the loading direction is parallel to the *c*-axis. The fracture

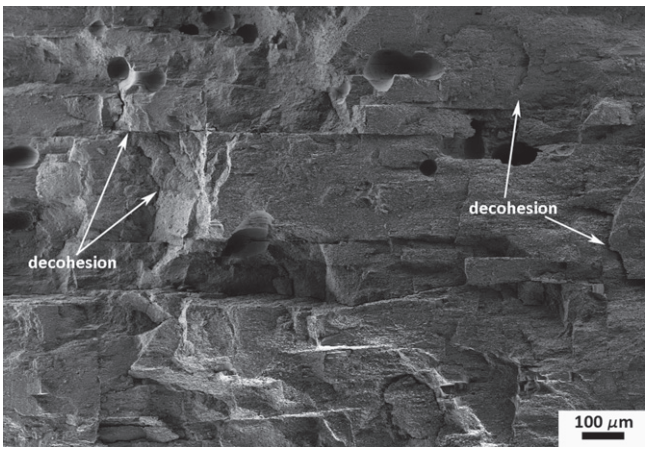

Figure 7. Fracture surface of the YBCO single grain after the three-point bending test for the measurement of flexural strength at 77 K. The loading direction was parallel to the *c*-axis. Decohesion and fracture of the domain are shown in the figure.

Figure 8. Fracture surface of YBCO single grain after the three-point bending test for the measurement of flexural strength at 77 K. The loading direction was parallel to the *ab*-plane. The propagation of the crack parallel to the *ab*-plane and the density of voids are indicated.

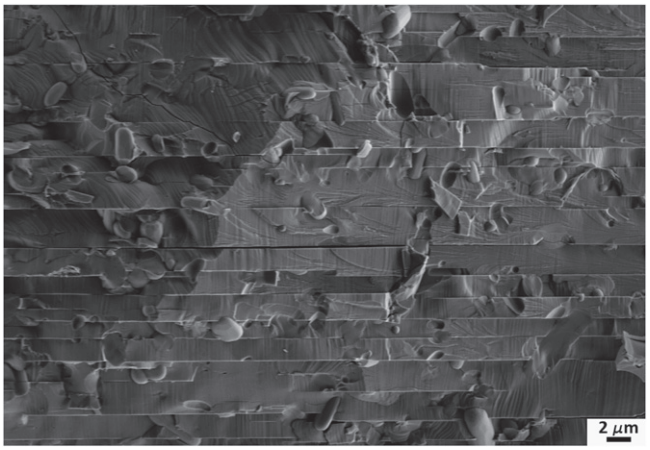

Figure 9. Fracture surface of GdBCO/Ag single grain after the three-point bending test for the measurement of the flexural strength at 77 K. The loading direction was parallel to the *c*-axis. A smooth fracture surface and the propagation of cracks perpendicular to the *ab*-plane are observed.

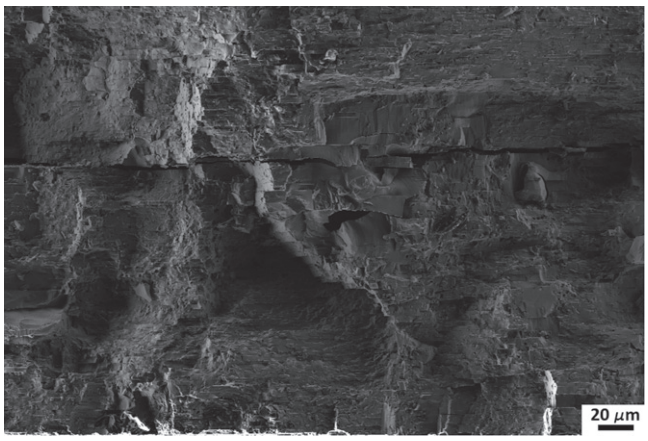

Figure 10. Fracture surface of GdBCO/Ag single grain after the three-point bending test for the measurement of flexural strength at 77 K. The loading direction was parallel to the *c*-axis. The fracture of the grain and the propagation of the crack parallel to the *ab*-plane are shown.

mechanics are controlled by the density of cracking when the loading direction is parallel to the *ab*-plane, whereas, for the other loading direction, the fracture depends on the crack density as well as on decohesion of the grain.

Figures 9 and 10 show the fracture surfaces of a GdBCO/Ag grain tested at 77 K for a loading direction parallel to the *c*-axis. These surfaces are much smoother than those observed for the YBCO single grain from the fractographic results. However, the presence of Ag particles reinforces the GdBCO single grain and leads to a higher fracture energy for the propagation of cracks, which results in a narrowing of the area between the cracks.

The fracture mechanics of the bulk samples are determined predominantly by the crack density when the loading direction is parallel to the *ab*-plane (figure 11), with cracks propagating through the pre-existing cracks and around the silver particles. The similar behavior observed between the two directions tested for GdBCO/Ag is due to the presence of the Ag particles and their homogeneous distribution within the single grain. This results directly in the formation of smaller cracks and an associated higher energy being necessary to fracture the grain.

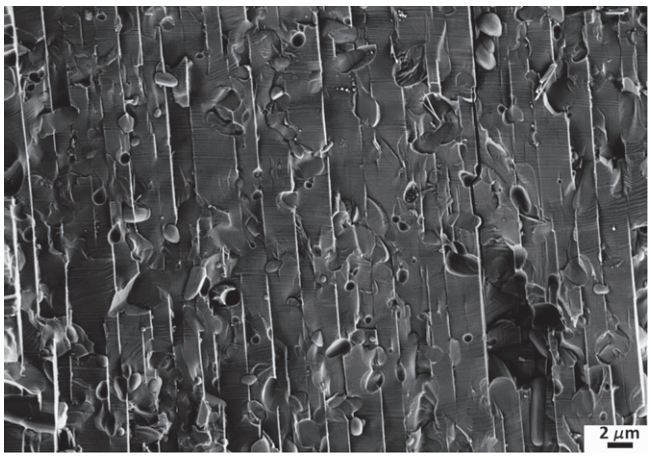

Figure 11. Fracture surface of GdBCO/Ag single grain after the three-point bending test for the measurement of flexural strength at 77 K. The loading direction was parallel to the *ab*-plane. Cracks propagate through the pre-existing microcracks and around the Gd-211 secondary phase inclusions.

3.3. Fracture toughness

Three-point bending tests on notched, prismatic samples were performed to determine the fracture toughness of both materials. Each notch, of nominal length of 35% of the thickness of the sample, was formed using a diamond thread (radius = 130 μm). The tests were performed for the two loading directions at temperatures of 300 and 77 K. Ten tests were performed for each measurement condition, with the results shown in figure 12.

Both materials exhibit higher fracture toughness at 77 K than at room temperature, as was expected, although the behavior of the GdBCO/Ag single grain is more isotropic than YBCO, with anisotropic behavior observed for the latter for the two loading directions employed. The fracture toughness of YBCO is 35% higher for the different loading directions at room temperature, whereas the observed differences in this parameter for the two loading directions at 77 K and room temperature for the GdBCO/Ag sample were negligible.

The fracture toughness of YBCO and GdBCO/Ag at 77 K is between 1.38 and 1.87 MPa $m^{1/2}$ and 2.12 and 2.06 MPa $m^{1/2}$, respectively. This significant difference is again due to the presence of Ag particles, which improves the mechanical properties and lead to more isotropic single grains with regard to their mechanical behaviour.

YBCO single grains exhibit similar behavior at 300 K for both loading directions. The fracture toughness for YBCO is much higher and closer to the values obtained for the GdBCO/Ag samples when the loading direction is parallel to the *ab*-plane. It can be concluded from the fracture surfaces

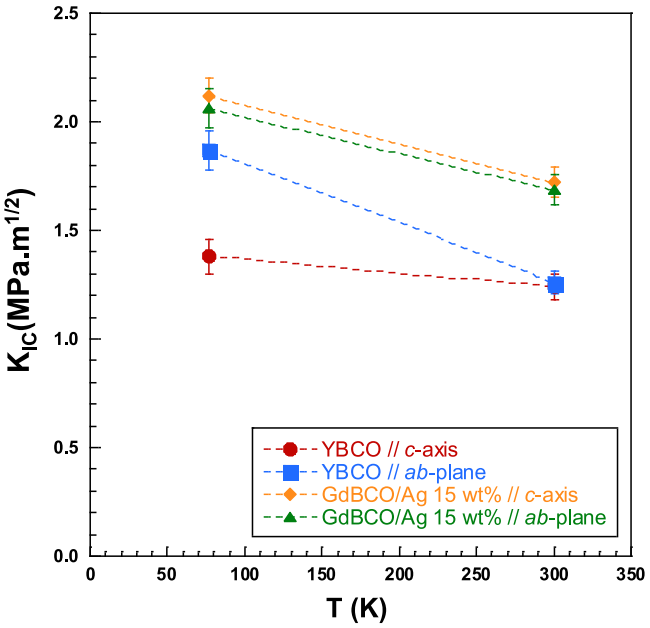

Figure 12. Variation of the fracture toughness as a function of temperature and loading direction. Each point represents the value of the mean of ten tests, and the bars indicate mean quadratic error.

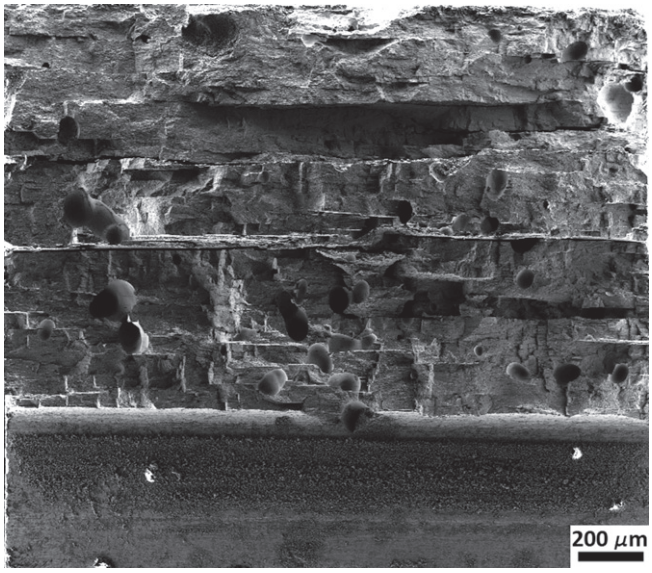

Figure 13. Fracture surface of the YBCO single grain after the three-point bending test for the measurement of fracture toughness at 77 K. The loading direction was parallel to the *c*-axis.

(figures 13 and 14) that, although the cracks propagate perpendicular to that of the main crack propagation plane, the presence of voids leads to decohesion of the grain.

Narrow regions between cracks can be observed that are similar in appearance to the fracture surfaces of the GdBCO/Ag samples for the *c*-axis loading direction (figure 15). A fractographic study of the fracture surfaces of the GdBCO/Ag single grains is shown in figures 16 and 17. In both cases, examination of the surfaces indicates that brittle fracture has occurred. It can be concluded from these experimental results that the propagation of cracks *perpendicular* to the *ab*-plane

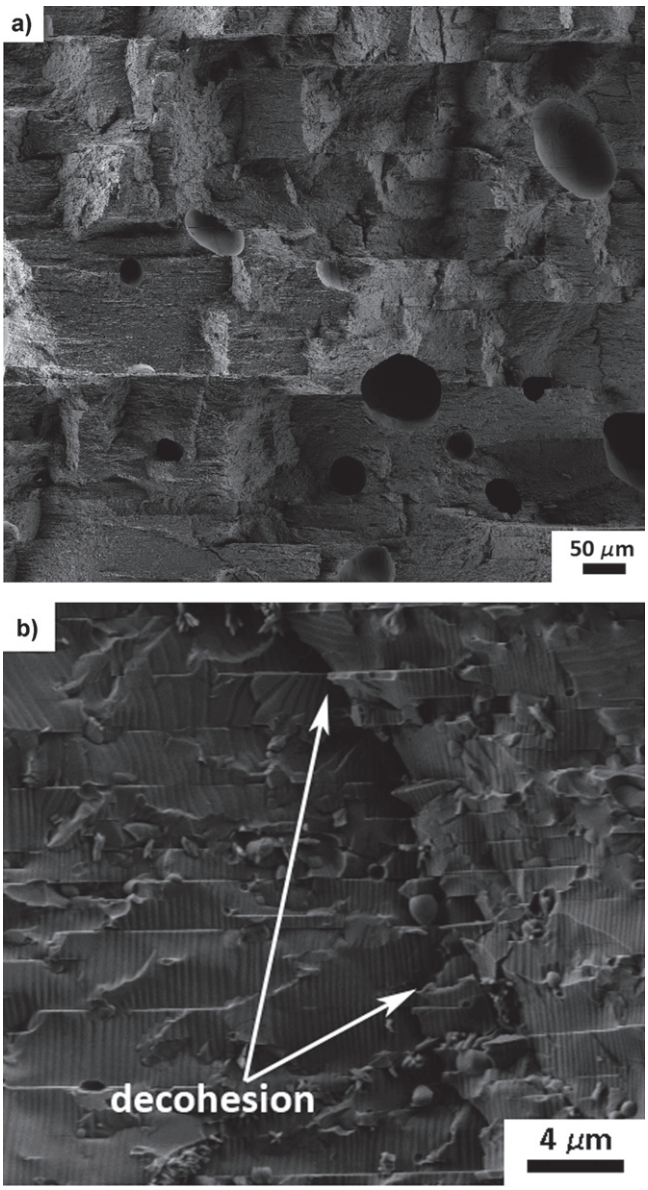

Figure 14. Fracture surface of the YBCO single grain after the three-point bending test for the measurement of fracture toughness at 77 K. The loading direction was parallel to the *c*-axis. (a) Propagation of the crack perpendicular to the *ab*-plane and (b) Decohesion of the grain.

requires a similar order of magnitude of fracture energy as that for crack propagation in the direction *parallel* to the *ab*-plane. The silver particles act as a barrier to the propagation of the cracks, which consequently improves the flexural strength of the samples and homogenizes their mechanical behavior.

3.4. Splitting tensile strength

Four splitting tensile tests were performed at 77 K for each single grain. The loading direction was parallel to the growth facet lines in order to measure the tensile strength of the grain at its weakest position, which is the limiting condition for the practical application of these materials. The results of this measurement are shown in table 1.

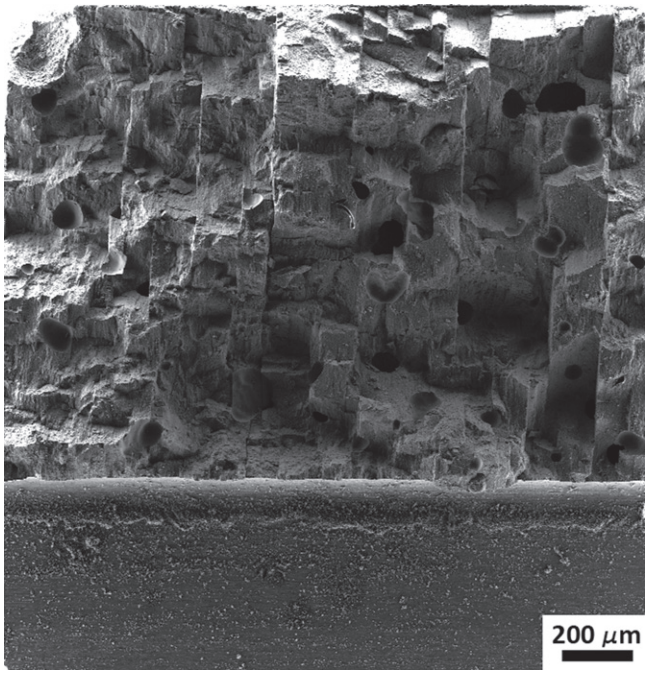

Figure 15. Fracture surface of the YBCO single grain after the three-point bending test for the measurement of fracture toughness at 77 K. The loading direction was parallel to the *ab*-plane. Brittle fracture and a curved fracture surface are observed.

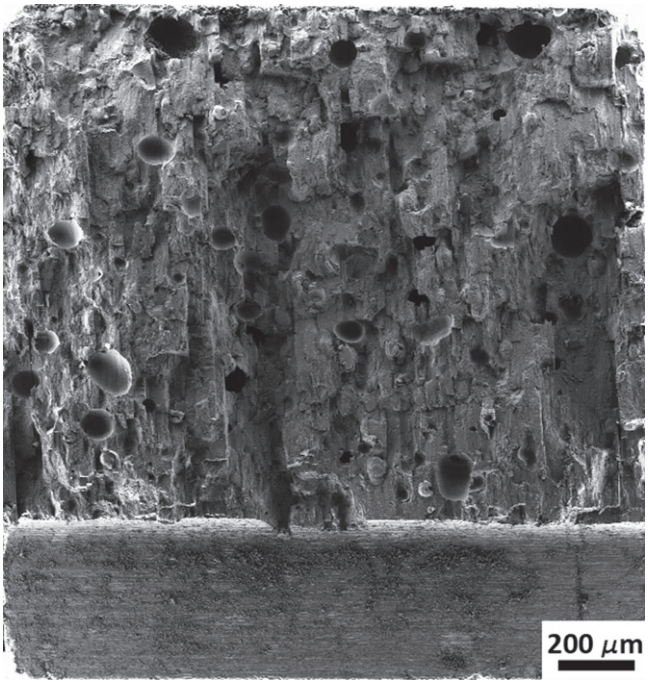

Figure 17. Fracture surface of GdBCO/Ag single grain after the three-point bending test for the measurement of fracture toughness at 77 K. The loading direction was parallel to the *ab*-plane. Brittle fracture and abrupt fracture surface is observed.

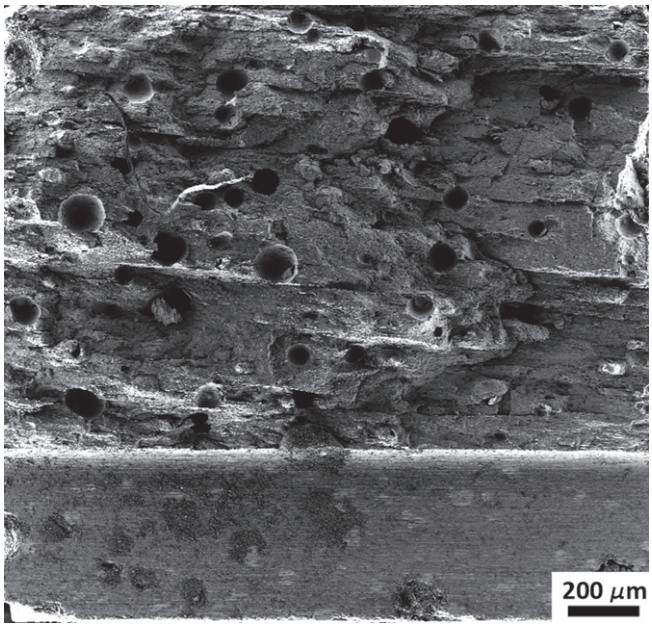

Figure 16. Fracture surface of GdBCO/Ag single grain after the three-point bending test for the measurement of fracture toughness at 77 K. The loading direction was parallel to the *c*-axis. A change in the direction of the propagation of the main crack is observed.

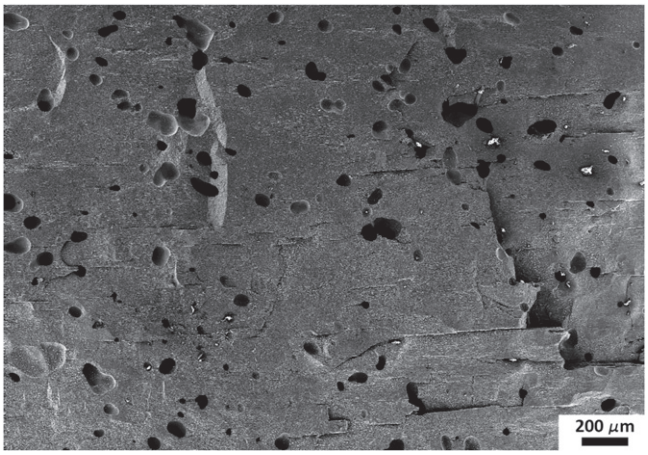

Figure 18. Fracture surface of the YBCO single grain after the splitting test at 77 K. The propagation of cracks parallel to the *ab*-plane and the density of voids can be seen.

Table 1. The splitting tensile strength determined by Brazilian tests at 77 K for YBCO and GdBCO/Ag 15 wt% cylindrical samples.

Material Sample name	σ_T (MPa) *F*//facet lines
YBCO	31 ± 3
GdBCO + Ag 15 wt%	34 ± 3

It has been observed that both grains exhibit a similar tensile strength at 77 K, with the measured value for GdBCO/Ag being slightly higher than that for YBCO. The resulting observed tensile strengths suggests that these tests are less sensitive to the presence of Ag than flexural strength or fracture-toughness measurements. The fracture, in this case, is

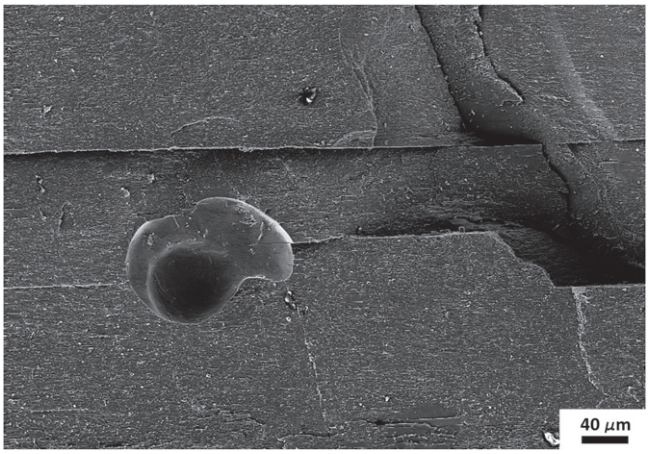

Figure 19. Fracture surface of the YBCO single grain after the splitting test at 77 K. Cracks propagate mainly parallel to the *ab*-plane, although perpendicular cracks that led to the fracture can be observed.

Figure 20. Fracture surface of the GdBCO/Ag single grain after the splitting test at 77 K. The propagation of the cracks is parallel to the *ab*-plane and the density of cracking produced narrow superconducting areas within the sample.

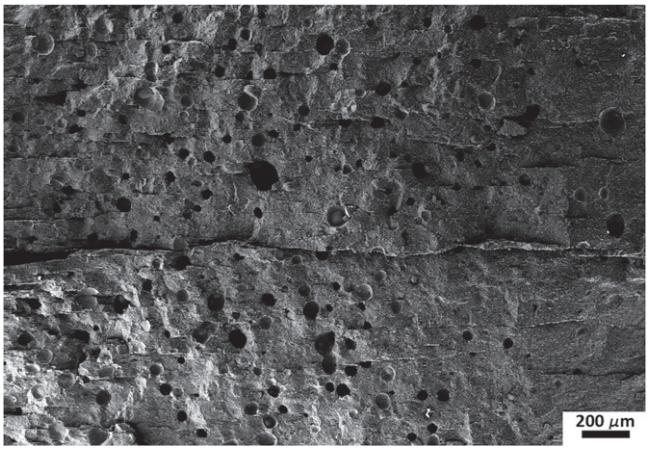

Figure 21. Fracture surface of the GdBCO/Ag single grain after the splitting test at 77 K. The propagation of the cracks is parallel to the *ab*-plane and the fracture is more abrupt than in the case of YBCO.

Table 2. Mean values of hardness and quadratic errors for the Vickers hardness tests at 300 K for different applied loads.

Loading direction	Material	Hv (GPa) $F = 0.98$ N	Hv (GPa) $F = 9.8$ N
//*c*-axis	YBCO	8.1 ± 0.2	6.7 ± 0.2
//*ab*-plane	YBCO	7.3 ± 0.2	6.1 ± 0.2
//*c*-axis	GdBCO + Ag 15 wt%	7.1 ± 0.2	—
//*ab*-plane	GdBCO + Ag 15 wt%	6.7 ± 0.2	4.5 ± 0.2

Table 3. Mean values of hardness and quadratic errors for the Vickers hardness tests at 77 K for different applied loads.

Loading direction	Material	Hv (GPa) $F = 0.98$ N	Hv (GPa) $F = 9.8$ N
//*c*-axis	YBCO	13.6 ± 0.3	9.9 ± 0.1
//*ab*-plane	YBCO	12.7 ± 0.4	7.9 ± 0.1
//*c*-axis	GdBCO + Ag 15 wt%	13 ± 1	7.5 ± 0.6
//*ab*-plane	GdBCO + Ag 15 wt%	10.7 ± 0.5	7.1 ± 0.2

controlled mainly by the presence of pre-existing cracks, with crack propagation occurring predominantly parallel to the *ab*-plane. The similarity of the results observed for the two materials can be also explained by taking into account their behavior during fracture-toughness measurements. K_{IC} for YBCO is 1.87 MPa $m^{1/2}$ at 77 K when the loading direction is parallel to the *ab*-plane, which is very close to the corresponding value for GdBCO/Ag (2.06 MPa $m^{1/2}$).

Figures 18 and 19 show the fracture surfaces of the YBCO samples after the splitting tests, which tend to be flatter than the fracture surfaces of the GdBCO/Ag single grains. Additionally, a wider region between cracks is observed, although the fracture mechanism for both samples is the same. The slightly different size of the voids between the YBCO and GdBCO/Ag samples is also apparent from these figures.

On the other hand, figures 20 and 21 show the propagation of the cracks parallel to the *ab*-plane for a loading direction parallel to the growth facet lines. An increase in density of narrow cracks can be observed following the fracture. The fracture mechanism is dominated by the presence and density of the pre-existing microcracks for both grains, which act as a path for the propagation of the crack during the tests. However, the tensile strength of the grains is relatively high (~30 MPa) taking in account the brittle nature of these compounds and the fact that they contain a variety of microstructural defects, such as voids and microcracks.

3.5. Hardness

The hardness on the nano- and micro-scale was studied via Vickers tests and nanoindentation, respectively. The results obtained at 300 K are presented in table 2. Table 3 shows the changes in hardness for the different loading directions and temperatures. It is well known that the hardness of (RE)BCO

Table 4. Hardness obtained by nano-indentation measurements at 300 K. The mean values and the quadratic mean errors are as indicated.

Loading direction	Material	Hardness (GPa)
//*c*-axis	YBCO	11.3 ± 0.2
//*ab*-plane	YBCO	10.9 ± 0.2
//*c*-axis	GdBCO + Ag 15 wt%	8.8 ± 0.3
//*ab*-plane	GdBCO + Ag 15 wt%	9.3 ± 0.1
	Ag	1 ± 0.1

single crystals is higher at 77 than at 300 K. An increase in hardness at 77 K and isotropic behavior are observed for both single grains. In all cases, the values for GdBCO/Ag are lower than those of YBCO due to the presence of the relatively soft silver particles. On the other hand, the nano-indentation measurements enabled the hardness of the Ag particles and the Y-123/Gd-123 phases to be determined directly (table 4). The much higher values are due to the smaller tip indenter that provides an opportunity to test the different phases (Y-123 or Gd-123, Y-211 or Gd-211, Ag) separately, in regions far from defects such as cracks and voids.

3.6. Elastic modulus

The elastic modulus, *E*, of the samples was studied by three different methods. Nano-indentation, grindosonic and three-point bending tests were performed at 300 K, with the normalized stress–strain curves used to determine *E* at 77 and 300 K. According to the literature, the most common method of obtaining the elastic modulus of (RE)BCO samples is by nano-indentation [25, 26]. However, this method is generally independent of the sample microstructure because the microstructure and the nano-indentation footprint are of a similar size. As a result, the values obtained by this measurement technique usually overestimate the actual macroscopic properties of the samples. Therefore, grindosonic measurements and calculation of *E* from the linear part of the load-displacement curves of the specimens were performed preferentially. Table 5 shows the mean values of *E* and the corresponding quadratic error in the measurements for each material, temperature and direction of the applied load. It can be observed that the values obtained by grindosonic and three-point bending tests are more similar, whereas measurements by nano-indentation tend to be slightly higher. This result is in good agreement with the observed macroscopic behavior of the grain, since the former methods include the defects of the material, whereas the latter depends predominantly on the behavior of the constituent phases. However, a difference between the values obtained by grindosonic and three-point bending tests at 300 K can be observed that is more significant in the case of the YBCO samples. The origin of this difference is due to the fact that during the three-point bending tests, all the defects (cracks and porosity) are taken into account, whereas in the case of the grindosonic method, only the porosity is taken into account. Therefore, lower values are anticipated in a three-point bending test than in a grindosonic test. Significantly, this difference is less clear for the GdBCO/Ag samples where shorter cracks and smaller voids are observed due to the presence of the Ag particles.

4. Conclusions

The mechanics of single-grain, bulk YBCO and GdBCO + 15 wt% Ag fabricated by top seeded melt growth have been studied for two directions of applied load at 77 and 300 K. The flexural strength and fracture toughness have been determined through three-point bending tests. The splitting tensile strength of the samples has been evaluated at 77 K by Brazilian tests and the hardness and elastic modulus have been measured.

The results obtained show that both single grains exhibit very good mechanical properties at 77 and 300 K. However, the intrinsic microstructural anisotropy within YBCO influences significantly the measured macroscopic properties of the bulk material, whereas the mechanical behavior of GdBCO/Ag is more homogeneous.

The fracture mechanics of both YBCO and GdBCO/Ag single grains have been studied by SEM. This indicates that the presence of Ag particles for GdBCO/Ag samples not only improves the mechanical properties, but also provides more homogeneous behavior, independent of the loading direction. Decohesion of the grain, on the other hand, was the main fracture mechanism observed for YBCO.

Finally, it can be concluded that the high quality of the single grains and their good mechanical performance at 77 K

Table 5. Young's modulus, *E*, measured by different methods. The values for *E* have been obtained by three-point bend tests at 77 K.

Temperature (K)	Loading direction	Material	Nano-indentation *E* (GPa)	Grindosonic *E* (GPa)	TPB tests *E* (GPa)
	//*c*-axis	YBCO	155 ± 1	120 ± 2	94 ± 7
	//*ab*-plane	YBCO	191 ± 1	126 ± 2	90 ± 6
300	//*c*-axis	GdBCO + Ag 15 wt%	146 ± 3	115 ± 2	100 ± 9
	//*ab*-plane	GdBCO + Ag 15 wt%	173 ± 1	99 ± 2	105 ± 6
		Ag	85 ± 1	—	—
	//*c*-axis	YBCO	—	—	157 ± 13
	//*ab*-plane	YBCO	—	—	145 ± 16
77	//*c*-axis	GdBCO + Ag 15 wt%	—	—	119 ± 11
	//*ab*-plane	GdBCO + Ag 15 wt%	—	—	103 ± 15

makes them potentially suitable for applications where the field-trapping capability needs to be enhanced.

Acknowledgments

The authors would like to acknowledge the Ministerio de Economia y Competitividad of Spain (MAT2012-38541-C02-02) for funding for this research project and the financial support of the UK Engineering and Physical Science Research Council (EPSRC). In addition, they would like to acknowledge the support of CEI Campus Moncloa in the provision of equipment for the microscopy analysis at the Materials Science Department of the Technical University of Madrid.

References

[1] Murakami M 1992 *Supercond. Sci. Technol.* **5** 185–203
[2] Campbell A M and Cardwell D A 1997 *Cryogenics* **37** 567
[3] Cardwell D A 1998 *Mater. Sci. Eng.* B **53** 1
[4] Shi Y, Hari Babu N, Lida K and Cardwell D A 2007 *Supercond. Sci. Technol.* **20** 38–43
[5] Yoo S I, Sakai N, Takaichi H, Higuchi T and Murakami M 1994 *Appl. Phys. Lett.* **65** 633–5
[6] Cardwell D A and Hari Babu N 2006 *Physica* C **1–7** 445–8
[7] Hari Babu N, Lo W, Cardwell D A and Campbell A M 1999 *Appl. Phys. Lett.* **75** 2981–3
[8] Nariki S, Sakai N, Murakami M and Hirabayashi I 2004 *Physica* C **412–414** 557–65
[9] Durrell J H *et al* 2014 *Supercond. Sci. Technol.* **27** 082001
[10] Nakiri S, Sakai N and Murakami M 2005 *Supercond. Sci. Technol.* **18** S126
[11] Sakai N, Seo S J, Inoue K, Miyamoto T and Murakami M 1999 *Advances in Superconductivity XI* vol 685–688 ed N Koshizuka and S Tajima (Tokyo: Springer)
[12] Yoshimo Y, Iwabuchi A, Noto K, Sakai N and Murakami M 2001 *Physica C: Supercond.* **357–360** 796–8
[13] Konstantopoulou K, Roa J J, Jiménez-Piqué E, Segarra M and Pastor J Y 2014 *Ceram. Int.* **40** 12797–806
[14] Okudera T, Murakami A, Katagiri K, Kasaba K, Shoji Y, Noto K, Sakai N and Murakami M 2003 *Physica* C **392–396** 628–33
[15] Shi Y, Hari Babu N, Iida K, Yeoh W K, Dennis A R and Cardwell D A 2009 *Supercond. Sci. Technol.* **22** 075025
[16] Rocco C, Guinea G V, Planas J and Elices M 2001 *Cement and Concrete Research* **31** 73–82
[17] Salazar A, Pastor J Y and Llorca J 2002 *Carbon* **40** 609–16
[18] Pastor J Y, Poza P and Llorca J 1999 *Journal of American Ceramic Society* **82** 3139–44
[19] Shi Y, Hari Babu N, Lida K, Yeoh W K, Dennis A R, Pathak S K and Cardwell D A 2010 *Physica* C **470** 685–8
[20] Shi Y, Hari Babu N and Cardwell D A 2005 *Supercond. Sci. Technol.* **18** L13
[21] Timoshenko S 1955 *Strength of Materials* 3rd edn (New York: D Van Nostrand Company)
[22] Guinea G, Pastor J Y, Planas J and Elices M 1998 Stress intensity factor, compliance and CMOD for a general three-point-bend beam *International Journal Fracture* **89** 103–16
[23] Oliver W C and Pharr G M 1992 *J. Mater. Res.* **7** 1564–83
[24] Hull J R and Murakami M 2004 *Proceeedings of the IEEE* **92**
[25] Yoshimo Y, Iwabuchi A, Noto K, Sakai N and Murakami M 2001 *Physica C. Supercond.* **357–360** 796–8
[26] Roa J J, Konstantopoulou K, Jiménez-Piqué E, Martin V, Segarra M and Pastor J Y 2012 *Ceram. Int.* **38** 2035–42